Desalination and Water Treatment
www.deswater.com

50 (2012) 387–396
December

doi: 10.1080/19443994.2012.720442

Taylor & Francis
Taylor & Francis Group

Estimation of convective heat transfer coefficient in a single-slope solar still: a numerical study

Nader Rahbar, Javad Abolfazli Esfahani*

Center of excellence on Modelling and Control Systems (CEMCS) &
Mechanical Engineering Department, Ferdowsi University of Mashhad, Mashhad 91755-1111, Iran
Tel. +98 511 8805005; Fax: +98 511 8763301; email: Abolfazl@um.ac.ir

Received 2 October 2011; Accepted 11 July 2012

ABSTRACT

The intention of this work is to investigate the natural convection effect in a 2-D single-slope solar still. The flow is assumed as steady, laminar, and incompressible ideal gas. A numerical model based on SIMPLEC algorithm is used for the solution of mass, momentum, energy, and concentration equations. The solutions are performed for several values of aspect ratio and Rayleigh number between 2.5 and 5.5 and between 5×10^6 and 5×10^7, respectively. Moreover, a new correlation for estimating the convective heat transfer coefficient has been obtained, which has a good agreement with published well-known models. The results show that, for a given aspect ratio, Rayleigh number has a direct effect on Nusselt number. On the other hand, for a fixed Rayleigh number, the value of Nusselt number decreases when the aspect ratio increases. Furthermore, it is found that the maximum heat transfer coefficient is in the area where flow directed downward from glass to water.

Keywords: CFD study; Single-slope solar still; Convective heat transfer coefficient; Aspect ratio; Rayleigh number

1. Introduction

Single-slope solar stills are one of the most well-known desalination facilities which use solar radiation for producing distilled water. They are cheap, simple, and have low maintenance. Solar radiation is also free, never lasting, and available on site. The performance evaluation of solar stills can be mainly classified into two categories: experimental and theoretical studies.

There are hundreds of studies which use experimental procedure either to set up various types or to improve the performance and productivity of solar stills. Hidouri et al. [1] reported that using double-glass cover provides more productivity than single-glass one. Phadatare and Verma [2] experimentally studied the effect of cover materials on the heat and mass transfer coefficients in solar stills. They reported that the solar still with glass cover produced 30% more output than the still with plastic cover. Esfahani and Rahbar [3,4] used thermoelectric technology to improve the still's productivity. More detail reviews can be found in the works done by Sampathkumar et al. [5], Kaushal and Varun [6], Mutasher et al. [7], and Balan et al. [8].

In addition of experimental researches, there are lots of studies which use mathematical modeling for productivity estimation of solar stills. Al-Hinai et al. [9] used a mathematical model to predict the effect of climatic and design parameters on the performance of a solar still. They concluded that the climatic conditions have a direct effect on productivity. They also showed that the initial water temperature and insulation thickness have direct effects, but the cover angle

*Corresponding author.

has an inverse effect in summer and a direct effect in winter. Abdenacer and Nafila [10] and Abu-Arabi et al. [11] showed that a better efficiency is obtained at a maximum temperature difference between water and glass cover. Tiwari et al. [12] showed that using a mathematical model based on inner glass temperature gives more accurate results in mathematical modeling of solar stills. There are also other mathematical studies on the effect of solar collector [13], modeling of a tubular solar still [14], the effects of water depth and glass angle [15,16], modeling of external reflectors [17], and parametric modeling of solar stills [18–20].

The main part of mathematical modeling is the solving of energy-balance equations between different parts of a solar still. The heat transfer in solar still is mainly classified into two categories: internal and external heat transfer. Internal heat transfer, which consists of radiation, convection, and evaporation, occurs between the water surface and the glass cover. However, radiation is independent of convection and evaporation, while convection and evaporation take place simultaneously and strongly depend on each other [5].

Natural convection in solar stills takes place because of the buoyant force arising from density difference due to the temperature and vapor concentration gradients between the water surface and the glass cover. This type of natural convection is called double-diffusive or thermosolutal convection [21–23]. The construction of experimental facilities for the investigation of simultaneous molecular diffusion and buoyant convection is extremely difficult and expensive. So, many researchers have been using computational fluid dynamics (CFD) to study the convection phenomena in solar stills. Rheinlander [24] used a finite-difference algorithm to solve the governing equations in a solar still. He showed a good agreement between the numerical and experimental results. Abu-Rayan and Djebedjian [25] conducted a theoretical investigation and reported that there exist some adjacent recirculating zones with opposite direction inside the enclosure. Papanicolaou and Belessiotis [21,26] used a CFD simulation to investigate the unsteady behavior of laminar and turbulent flow regime in an asymmetric trapezoidal enclosure. They reported that the number of multicellular flow field depends on the Rayleigh number and geometry. Omri et al. [27] studied the flow structure sensitivity to the flow parameters, Rayleigh number, and tilt-angle in a triangular cavity. Murase et al. [28] compared a tube-type with a conventional flat-basin solar still by a numerical analysis. They concluded that the tube-type produced a larger convection area than a conventional flat one. Chouikh et al. [29] numerically studied the heat and mass transfer phenomena in an inclined glazing cavity. They proposed that the existence of a single rotating cell is the best flow structure for enhancing the productivity.

As mentioned before, the calculation of heat transfer coefficient is the main object in estimating the heat transfer in a solar still. The most well-known relation for heat transfer coefficient is a semi-empirical equation proposed by Dunkle [30]. Moreover, some other models have been proposed in the literature [31–36]. In an experimental study, Tiwari and Dwivedi [37] showed that Dunkle's model gives better agreement between the experimental and theoretical data. However, Dunkle's model has some limitations [30]:

(1) It is independent of cavity volume.
(2) It was proposed based on experimental data for a low operating temperature range between 55 and 70°C.
(3) The mean temperature difference between water and glass is 11°C.
(4) The slope of the glass cover was small (10°), so condensing and evaporating surfaces were approximately parallel.
(5) It was originally developed for free convection of air without evaporation [38].

Clark [39] gave a new experimental model for higher operating ranges. He observed that in a steady-state condition, the constant of his model was half of Dunkle's model due to equal evaporation and condensation rate. In another experimental study, Shawaqfeh and Farid [38] evaluated the accuracy of Dunkle's model. It was observed that the Dunkle's model overestimates the evaporation by 30%. They proposed two empirical correlations based on Bulk Motion and Chilton–Colburn analogy for estimating the convective heat transfer coefficient. However, their correlations were independent of still geometry similar to Dunkle's model.

The heat transfer coefficient is a significant issue in designing of a solar still. So, it requires more work to find insight of the process and to obtain a more accurate correlation to estimate the output of a solar still. The aim of this research is to construct a numerical procedure for evaluating and studying the fluid structure inside a single-slope solar still. Moreover, a new correlation for the convective heat transfer coefficient is proposed as a function of still geometry.

2. Theoretical background

The convective heat transfer takes place in the form of double-diffusive natural convection inside

solar stills. In the following sections, we describe the various thermal models and the method of numerical analysis used to study the nature of convective heat transfer in a single-slope solar still.

2.1. Thermal models

Natural convection in solar stills takes place because of the buoyant force caused by density variation due to the temperature and concentration gradients. The rate of convective heat transfer between the water and glass is given by:

$$q_c = h_{c,w-g} A_g (T_w - T_g) \quad (1)$$

The convective heat transfer coefficient $h_{c,w-g}$ is a function of fluid properties, still geometry, flow characteristics, and operating temperature. Various experimental models have been proposed to evaluate the internal heat transfer coefficients which are given as follows:

2.1.1. Jakob's model

This model is used for estimating the heat transfer coefficient for a laminar flow in a horizontal square cavity [40]:

$$\mathrm{Nu} = 0.068\mathrm{Ra}^{1/3}, 4 \times 10^5 < \mathrm{Ra} < 10^7, 0.5 \le \mathrm{Pr} \le 2 \quad (2)$$

where

$$\mathrm{Ra} = \frac{\rho^2 g \beta C_p H^3 \Delta T}{\mu k} \quad (3)$$

2.1.2. Dunkle's model

The most widely used equation for calculating the heat transfer coefficient was given by Dunkle [41]. This model is based on Sharpley and Boelter [42] and Jakob relations:

$$h_{c,w-g} = 0.884(\Delta T')^{1/3} \quad (4)$$

where

$$\Delta T' = \left[(T_w - T_{gi}) + \frac{(P_w - P_{gi})(T_w + 273)}{2689000 - P_w}\right] \quad (5)$$

$$P_w = \exp\left(25.317 - \frac{5144}{T_w + 273}\right) \quad (6)$$

$$P_{gi} = \exp\left(25.317 - \frac{5144}{T_{gi} + 273}\right) \quad (7)$$

Another form of Dunkle's model is:

$$\mathrm{Nu} = 0.075(\mathrm{Ra}')^{1/3} \quad (8)$$

where

$$\mathrm{Ra}' = \frac{\rho^2 g \beta C_p H^3 \Delta T}{\mu k} \quad (9)$$

In above equations, the properties of humid air are calculated by the equations given in Table 1 note that, $T_i = (T_g + T_w)/2$ and $H = (H_l + H_r)/2$.

In another study, Tsilingiris [43] reported that in high Rayleigh numbers, the coefficient of $C = 0.075$ in Dunkle's model must be replaced by $C = 0.05$. This

Table 1
Properties of humid air in terms of mean operating temperature [37]

Quantity	Expression
Specific heat, C_p	$999.2 + 0.1434 \times T_i + 1.101 \times T_i^2 - 6.758 \times 10^{-8} \times T_i^3$
Density ρ	$353.44/(T_i + 273.15)$
Thermal conductivity, k	$0.0244 + 0.7673 \times 10^{-4} \times T_i$
Viscosity, μ	$1.718 \times 10^{-5} + 4.62 \times 10^{-8} \times T_i$
Latent heat of vaporization of water, h_{fg}	$3.2615 \times 10^6 \times [1 - (7.616 \times 10^{-4} \times T_i)]$ for $T_i > 70$ $2.4935 \times 10^6 \times [1 -$ $(9.4749 \times 10^{-4} \times T_i + 1.3132 \times 10^{-7} \times T_i^2 - 4.7947 \times 10^{-9} \times T_i^3)]$ for $T_i < 70$
Partial saturated pressure at glass temperature, P_g	$\exp(25.317 - 5144)/(T_g + 273)$
Partial saturated pressure at water temperature, P_w	$\exp(25.317 - 5144)/(T_w + 273)$
Expansion factor, β	$1/(T_i + 273)$

was especially true in solar stills with a temperature range higher than 55˚C.

2.1.3. Corcione's model

Based on the numerical analysis, Corcione [44] proposed the following relation for a horizontal square cavity with different aspect ratios:

$$\mathrm{Nu}_{\mathrm{floor}} = \mathrm{Nu}_{\mathrm{ceiling}} = 0.21\left(\frac{L}{H}\right)^{0.09}\mathrm{Ra}^{0.25} \tag{10}$$

2.1.4. Shawaqfeh's model

In an experimental study, Shawaqfeh and Farid [38] showed that, Dunkle's model overpredicts the evaporation rate of water. They proposed two empirical correlations, based on Bulk Motion and Chilton–Colburn analogy, and showed that, with an accurate estimation of plate absorptance, glass transmittance, and wind loss, the accuracy of their model is better than Dunkle's model. The empirical correlations are given as follows:

$$\mathrm{Nu}_{\mathrm{bm}} = 0.057\mathrm{Ra}'^{1/3} \quad \text{Bulk-motion model} \tag{11}$$

$$\mathrm{Nu}_{\mathrm{cc}} = 0.051\mathrm{Ra}'^{1/3} \quad \text{Chilton–Colburn analogy} \tag{12}$$

where Ra´ is calculated by Eq. (9).

2.2. Mathematical formulation

A single-slope solar still with length of L and different heights of H_l and H_r is shown in Fig. 1, where the flow is assumed as two-dimensional, steady, and laminar. The bottom and top temperatures are assumed constant at T_w and T_g, while both side walls are adiabatic. The fluid is considered as humid air, incompressible ideal gas with constant physical properties and negligible viscous dissipation.

By above assumptions, the governing equations, which consist of conservation equations of mass, momentum, energy, and concentration, are given as follows [45,46]:

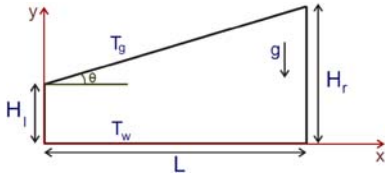

Fig. 1. Sketch of the geometry and coordinate system of the solar still.

$$\frac{\partial u}{\partial x} + \frac{\partial v}{\partial y} = 0 \tag{13}$$

$$\rho\left(u\frac{\partial u}{\partial x} + v\frac{\partial u}{\partial y}\right) = -\frac{\partial p}{\partial x} + \mu\left(\frac{\partial^2 u}{\partial x^2} + \frac{\partial^2 u}{\partial y^2}\right) \tag{14}$$

$$\rho\left(u\frac{\partial v}{\partial x} + v\frac{\partial v}{\partial y}\right) = -\frac{\partial p}{\partial y} + \mu\left(\frac{\partial^2 v}{\partial x^2} + \frac{\partial^2 v}{\partial y^2}\right) + \rho g_y \tag{15}$$

$$\rho C_{\mathrm{p}}\left(u\frac{\partial T}{\partial x} + v\frac{\partial T}{\partial y}\right) = k\left(\frac{\partial^2 T}{\partial x^2} + \frac{\partial^2 T}{\partial y^2}\right) \tag{16}$$

$$\left(u\frac{\partial \omega_{\mathrm{A}}}{\partial x} + v\frac{\partial \omega_{\mathrm{A}}}{\partial y}\right) = D_{\mathrm{AB}}\left(\frac{\partial^2 \omega_{\mathrm{A}}}{\partial x^2} + \frac{\partial^2 \omega_{\mathrm{A}}}{\partial y^2}\right) \tag{17}$$

The boundary conditions are:

$$\text{at top}: u = 0, v = 0, T = T_{\mathrm{g}}, \omega_{\mathrm{A}} = \omega|_{T=T_{\mathrm{g}},\varphi=100\%}$$

$$\text{at bottom}: u = 0, v = 0, T = T_{\mathrm{w}}, \omega_{\mathrm{A}} = \omega|_{T=T_{\mathrm{w}},\varphi=100\%} \tag{18}$$

$$\text{at both sides}: u = 0, v = 0, \frac{\partial T}{\partial x} = 0, \frac{\partial \omega_{\mathrm{A}}}{\partial x} = 0$$

Note that, in above equations, it is assumed that the buoyancy term is only due to thermal effect and not to concentration gradients. Moreover, the laminar regime is used to simplify the governing equations and solving procedure. As seen later, these assumptions have a reasonable agreement with experimental data published earlier in the literature, especially at low Rayleigh numbers.

3. Solution procedures

A system of discretized equations is obtained by integrating the governing differential Eqs. (13)–(17) over an elementary control volume. For the convection—diffusion formulation, first-order upwind scheme is used, while pressure–velocity coupling is handled by using SIMPLEC algorithm (semi implicit method for pressure linked equations corrected) described by Patankar [47,48]. The discretized equations are solved iteratively using a line-by-line Thomas algorithm.

The solution is considered to be fully converged when the values of scaled residuals are smaller than a prescribed value, 10^{-3}, except the energy equation, 10^{-6}. After the convergence is attained, the average Nusselt number $\overline{\mathrm{Nu}}$ is calculated by:

$$\overline{\mathrm{Nu}} = \frac{-H}{L(T_w - T_g)} \int_0^L \left.\frac{\partial T}{\partial n}\right|_{\mathrm{wall}} dx \tag{19}$$

The temperature gradient is calculated by assuming a first-order temperature profile along each wall node and adjacent interior node. The integral is approximated by the trapezoid rule.

Grid-dependency tests have been done for all the configurations investigated. The grid independency is attained when the percent changes of the average Nusselt numbers $\overline{\mathrm{Nu}}$ are smaller than a given accuracy value of 5%. Typical numbers of nodal points are 120×60. Fig. 2 shows the plot of grid-dependency check for a solar still with $\theta = 20^{\circ}$. Furthermore, in order to validate the numerical code, the solution obtained has been compared with the experimental data of the study of Shawaqfeh and Farid [38]. Table 2 shows the geometry used in validation of the CFD code. Fig. 3 shows the comparison between the numerical and experimental results. It can be concluded that there exist a very good agreement between the numerical and experimental results, especially with the Chilton–Colburn analogy reported by Shawaqfeh and Farid [38]. Fig. 3 also shows that the results of Dunkle's model are approximately 50% higher than those of numerical results, which is in accordance with the report of Shawaqfeh and Farid [38].

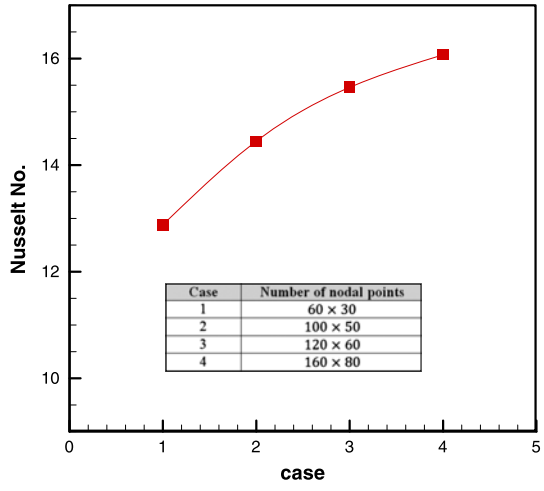

Fig. 2. Grid dependency check for a solar still with $\theta = 20^{\circ}$.

Table 2
Geometry of solar still used for validation of code [38]

L	H_l	H_r	Inclination angle
0.98	0.1	0.47	20°

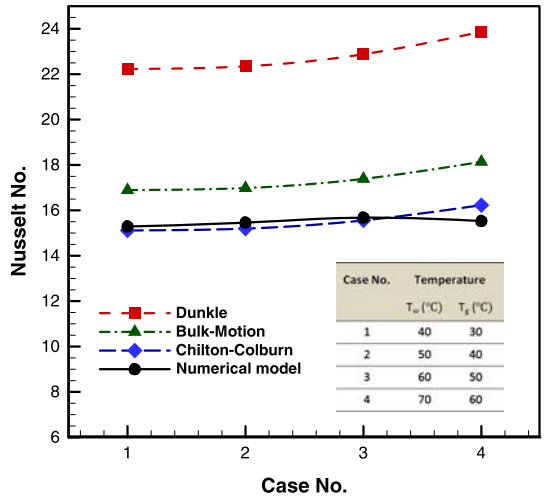

Fig. 3. Comparison between numerical simulation and reported experimental results [38].

4. Results and discussion

Numerical simulations are performed for various water and glass temperatures and different glass inclination angles. In this manner, it is possible to have different values of Rayleigh number and aspect ratio in the range of $5 \times 10^6 < \mathrm{Ra} < 5 \times 10^7$ and $2.5 \leq A \leq 5.5$, respectively. Table 3 shows different solar still configurations used for numerical calculations and relevant Nusselt numbers calculated by numerical modeling. Fig. 4 shows the flow streamlines in a typical solar still. It is seen that every two adjacent zones have flow streams with opposite directions.

The contours of temperature and water mass fraction are shown in Figs. 5 and 6. It is seen that, in the middle of recirculating zones, there are negligible changes in temperature and concentration of humid air. However, due to condensation and evaporation phenomena, there is rapid change in the fluid properties near the water surface and the glass cover. Also, a thermal plume with temperature of 307 K is directed downwards, while the mass fraction plume with 0.038 is moving upwards and with 0.036 is directed downwards. Moreover, it is concluded that in most parts of the area, the temperature and mass fraction variations are 1 K and 0.02, respectively.

Table 3
Different configurations of solar still used for the numerical simulation

Case No.	Temperature		Inclination angle (°)	Dimensions			A	Nu	$Ra \times 10^{-6}$
	T_w (°C)	T_g (°C)		H_l (m)	H_r (m)	L (m)			
1	40	30	20	0.1	0.47	0.98	3.44	15.29	26.03
2	50	40	20	0.1	0.47	0.98	3.44	15.46	26.45
3	60	50	20	0.1	0.47	0.98	3.44	15.68	28.39
4	70	60	20	0.1	0.47	0.98	3.44	15.53	32.22
5	40	30	10	0.1	0.27	0.98	5.3	11.43	7.12
6	50	40	10	0.1	0.27	0.98	5.3	12.74	7.23
7	60	50	10	0.1	0.27	0.98	5.3	12.8	7.76
8	40	30	30	0.1	0.66	0.98	2.58	22.26	21.76
9	50	40	30	0.1	0.66	0.98	2.58	23.35	21.83

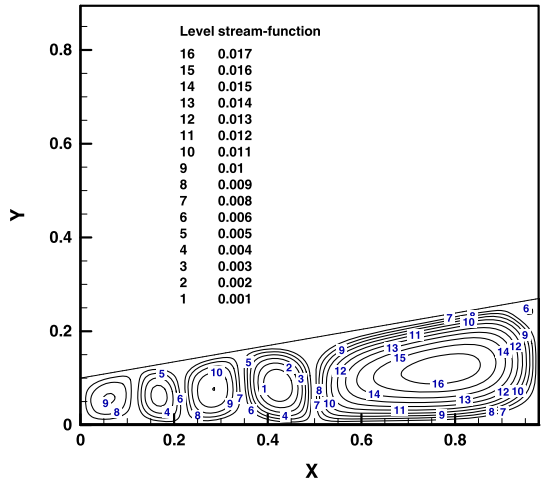

Fig. 4. Flow streamlines in a typical solar still, $Ra = 2.6 \times 10^7$ and $A = 3.44$.

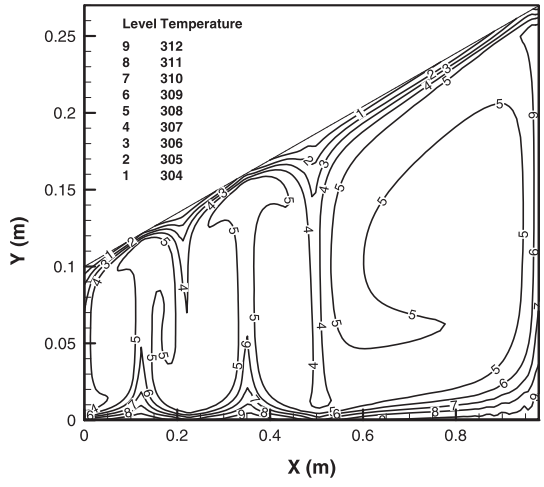

Fig. 5. Isotherms, $Ra = 2.6 \times 10^7$ and $A = 3.44$.
Note: The x–y axis has different scales.

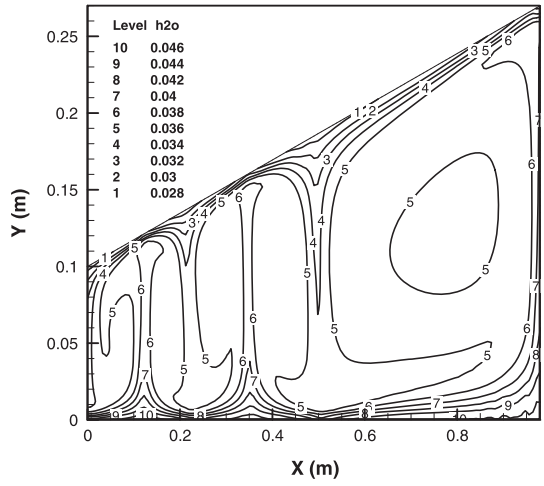

Fig. 6. Contours of water mass fraction, $Ra = 2.6 \times 10^7$ and $A = 3.44$.
Note: The x–y axis has different scales.

4.1. Heat transfer dimensionless correlations

Based on the general form of Corcione's Model [44], the numerical results obtained for the average Nusselt number, defined in Eq. (19), can be correlated as follows:

$$Nu = CRa^n A^m \tag{20}$$

In above equation, the values of coefficient C and the exponents n and m can be evaluated by the least square method through a logarithmic multiple regression procedure [49]. The dimensionless equation obtained from the best fit of data is listed below:

$$Nu = 0.28Ra^{0.25}A^{-0.16} \quad 5 \times 10^6 < Ra < 5 \times 10^7, 2.5 \leq A \leq 5.5, \ 10^\circ \leq \theta \leq 30^\circ, R^2 = 0.9 \tag{21}$$

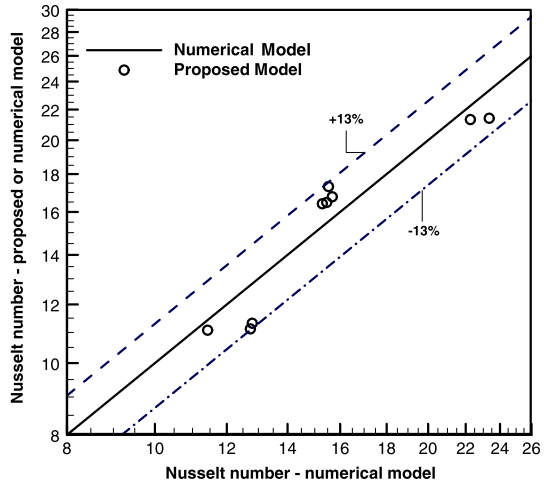

Fig. 7. Comparison between the results of proposed model (Eq. (21)) and numerical model.

In Eq. (21), the values of Rayleigh number should be calculated by properties of humid air given in Table 1. The comparison between the values of Eq. (21), numerical modeling, Bulk-motion, and Chilton–Colburn relations is shown in Figs. 7 and 8. Fig. 7 represents that the prediction of Eq. (21) has a maximum deviation of 12.5% from numerical results. Fig. 8 also shows that the prediction of Eq. (21) is closer to Bulk-motion than Chilton–Colburn's relation. The maximum deviation of proposed model from Chilton–Colburn and Bulk-motion is 12.5 and 5.5%, respectively.

4.2. Effects of aspect ratio and Rayleigh number

Fig. 9 shows the effects of Rayleigh number and aspect ratio on the variation of Nusselt number

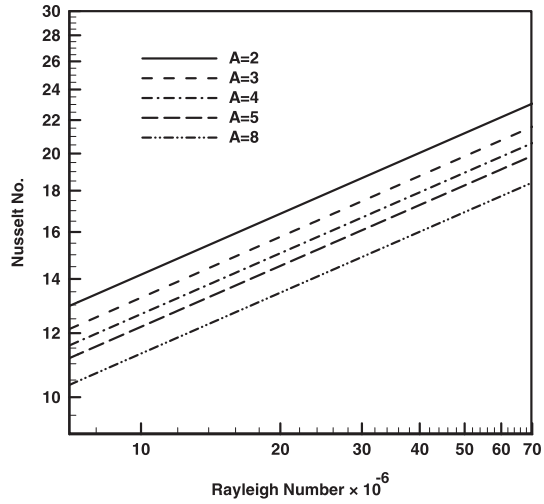

Fig. 9. Effects of Rayleigh number and aspect ratio on the value of Nusselt number.

calculated by Eq. (21). It is concluded that, in a fixed aspect ratio, the Rayleigh number has a direct effect on Nu number because of increasing of the convective flow intensity. On the other hand, for a fixed Rayleigh number, increasing of aspect ratio decreases the value of Nusselt number.

The variation of v-velocity, at the height of $y = 0.05$ m above the water surface, in two solar stills with the same Rayleigh Number and different aspect ratios, is shown in Figs. 10 and 11. The values of $v_y < 0$ imply the moving of airflow from glass to water, while the values of $v_y > 0$ mean the upward direction of flow from water to glass cover. In this manner, it is possible to find the number of recirculating zones inside the solar still. It can be concluded that, in a

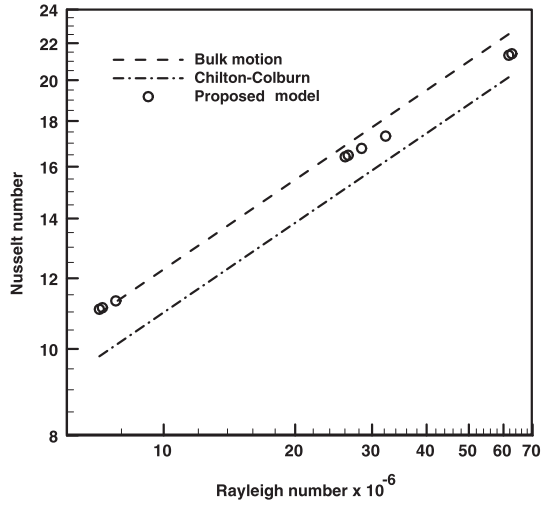

Fig. 8. Comparison between the results of proposed, Bulk-motion, and Chilton–Colburn models.

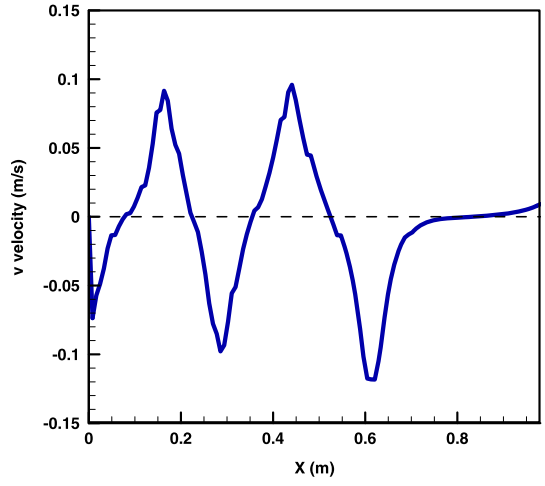

Fig. 10. Variation of v-velocity at $y = 0.05$ m, $A = 3.44$, and $\mathrm{Ra} = 2.6 \times 10^7$.

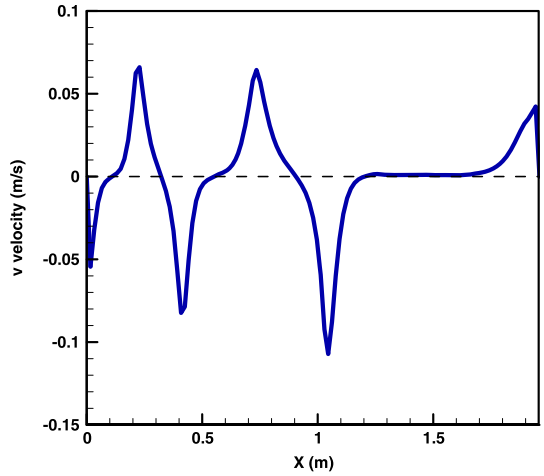

Fig. 11. Variation of v-velocity at $y = 0.05$ m, $A = 6.88$, and $\mathrm{Ra} = 2.6 \times 10^7$.

fixed Rayleigh number (with a fixed ΔT and H) and different aspect ratios (different values of L), the number of recirculating zones remains constant. However, the length of each zone increases by increasing of the aspect ratio. This reduces the upward movement of flow and decreases the value of Nusselt number.

4.3. Effect of velocity components

The effect of v-velocity on the convective heat transfer coefficient in a typical solar still is shown in Figs. 12 and 13. Fig. 12 shows that the maximum heat transfer coefficient is in the area where flow directed downward from glass to water (at $x = 0.02$ m, $x = 0.22$ m, and $x = 0.5$ m). In reference to Fig. 13, the

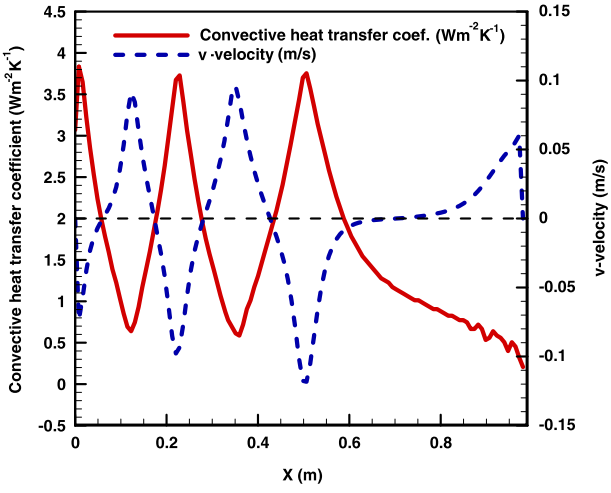

Fig. 12. Variation of v-velocity and convective heat transfer coefficient at $y = 0.05$ m, $A = 3.44$, and $\mathrm{Ra} = 2.6 \times 10^7$.

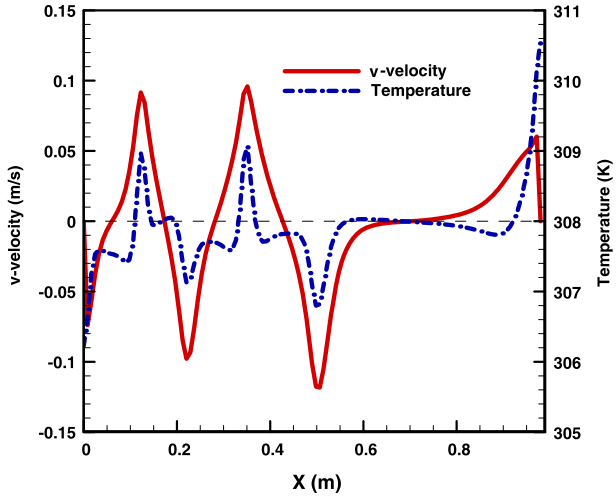

Fig. 13. Variation of v-velocity and temperature at $y = 0.05$ m, $A = 3.44$, and $\mathrm{Ra} = 2.6 \times 10^7$.

air temperature in these regions is low, so the rate of heat transfer and consequently the heat transfer coefficient are at their maximum values.

5. Conclusions

In this study, natural convection heat transfer phenomena in a typical single-slope solar still have been numerically studied. The values of aspect ratio and Rayleigh Number are between 2.5 and 5.5 and between 5×10^6 and 5×10^7, respectively. The main results obtained may be summarized as follows:

- Based on the numerical results, a relation of $\mathrm{Nu} = 0.28\mathrm{Ra}^{0.25}A^{-0.16}$ has been proposed for estimating the heat transfer coefficient which has a good agreement with published experimental correlations.
- For a given aspect ratio, the heat transfer coefficient increases with increasing of the Rayleigh number.
- For a given Rayleigh number, aspect ratio has an inverse effect on the heat transfer coefficient.
- The maximum heat transfer coefficient is in the area where the air moves downward from the glass cover to the water surface.
- By increasing the length of recirculating zones at a fixed Rayleigh number, the convective heat transfer coefficient decreases.
- In the middle of recirculating zones, there are negligible changes in temperature and concentration of humid air, extending over most of the solar still area.

Nomenclature

A_s	—	area of the solar still, (m^2)
A	—	aspect ratio, $A = L/H$
C_p	—	specific heat, $J\,kg^{-1}\,K^{-1}$
D_i	—	mass diffusivity of component i, $m^2\,s^{-1}$
H_l	—	height of the left side of solar still, m
H_r	—	height of the right side of solar still, m
H	—	specific height of solar still, $H = (H_l + H_r)/2$, (m)
$h_{c,w-g}$	—	convective heat transfer coefficient, $Wm^{-2}\ K^{-1}$
i_i	—	enthalpy of component i, $J\,kg^{-1}$
k	—	thermal conductivity, $Wm^{-1}\,K^{-1}$
L	—	length of the solar still, m
Nu	—	Nusselt number
u	—	x-component of velocity, $m\,s^{-1}$
v	—	y-component of velocity, $m\,s^{-1}$
P_w	—	partial pressure of the vapor at water temperature, Pa
P_{gi}	—	partial pressure of the vapor at glass temperature, Pa
q_c	—	convective heat transfer, W
Ra	—	Rayleigh number
T_w	—	water temperature, ℃
T_g	—	glass temperature, ℃
T_i	—	mean operating temperature, ℃
ΔT	—	temperature difference between water and glass, ℃

Greek symbols

β	—	volume expansion coefficient $\beta = 1/T$, (K^{-1})
ρ	—	density, $kg\,m^{-3}$
μ	—	viscosity, $Ns\,m^{-2}$
θ	—	inclination angle
ω_i	—	mass fraction of component, i

Subscripts

a	—	air
c	—	convective
g	—	glass
n	—	normal direction to the surface
s	—	still
v	—	vapor
w	—	water

References

[1] N. Hidouri, K. Hidouri, R.B. Slama, S. Gabsi, Effects of the simple/double glass cover use and the orientation of a simple solar still on operating parameters, Desalin. Water Treat. 36 (2011) 383–391.

[2] M. Phadatare, S. Verma, Effect of cover materials on heat and mass transfer coefficients in a plastic solar still, Desalin. Water Treat. 2 (2009) 248–253.

[3] J.A. Esfahani, N. Rahbar, M. Lavvaf, Utilization of thermoelectric cooling in a portable active solar still—an experimental study on winter days, Desalination 269 (2011) 198–205.

[4] N. Rahbar, J.A. Esfahani, Experimental study of a novel portable solar still by utilizing the heatpipe and thermoelectric module, Desalination 284 (2012) 55–61.

[5] K. Sampathkumar, T.V. Arjunan, P. Pitchandi, P. Senthilkumar, Active solar distillation–a detailed review, Renew. Sustain. Energy Rev. 14 (2010) 1503–1526.

[6] A. Kaushal, Varun, Solar stills: A review, Renew. Sustain. Energy Rev. 14 (2010) 446–453.

[7] S.A. Mutasher, N. Mir-Nasiri, S. Wong, K. Ngoo, L. Wong, Improving a conventional greenhouse solar still using sun tracking system to increase clean water yield, Desalin. Water Treat. 24 (2010) 140–149.

[8] R. Balan, J. Chandrasekaran, S. Shanmugan, B. Janarthanan, S. Kumar, Review on passive solar distillation, Desalin. Water Treat. 28 (2011) 217–238.

[9] H. Al-Hinai, M.S. Al-Nassri, B.A. Jubran, Effect of climatic, design and operational parameters on the yield of a simple solar still, Energy Convers. Manage. 43 (2002) 1639–1650.

[10] P.K. Abdenacer, S. Nafila, Impact of temperature difference (water-solar collector) on solar-still global efficiency, Desalination 209 (2007) 298–305.

[11] M. Abu-Arabi, Y. Zurigat, H. Al-Hinaib, Modeling and performance analysis of a solar desalination unit with double-glass cover cooling, Desalination 143 (2002) 173–182.

[12] G.N. Tiwari, S.K. Shukla, I.P. Singh, Computer modeling of passive/active solar stills by using inner glass temperature, Desalination 154 (2003) 171–185.

[13] B. Bacha, T. Dammak, B. Abdalah, Desalination unit coupled with solar collectors and a storage tank: Modeling and simulation, Desalination 206 (2007) 341–352.

[14] A. Ahsan, T. Fukuhara, Mass and heat transfer model of tubular solar still, Sol. Energy 84 (2010) 1147–1156.

[15] R. Tripathi, G.N. Tiwari, Thermal modeling of passive and active solar stills for different depths of water by using the concept of solar fraction, Sol. Energy 80 (2006) 956–967.

[16] H.S. Aybar, H. Assefi, Simulation of a solar still to investigate water depth and glass angle, Desalin. Water Treat. 7 (2009) 35–40.

[17] A. El-Sebaii, M. Al-Dossari, A mathematical model of single basin solar still with an external reflector, Desalin. Water Treat. 26 (2011) 250–259.

[18] M.A. Antar, S.M. Zubair, Performance evaluation of a solar still in the Eastern Province of Saudi Arabia—an improved analysis, Desalin. Water Treat. 22 (2010) 100–110.

[19] S.K. Shukla, V.P.S. Sorayan, Thermal modeling of solar stills: An experimental validation, Renew. Energy 30 (2005) 683–699.

[20] G.N. Tiwari, V. Dimri, A. Chel, Parametric study of an active and passive solar distillation system: Energy and exergy analysis, Desalination 242 (2009) 1–18.

[21] E. Papanicolaou, V. Belessiotis, Double-diffusive natural convection in an asymmetric trapezoidal enclosure: Unsteady behavior in the laminar and the turbulent-flow regime, Int. J. Heat Mass Transf. 48 (2005) 191–209.

[22] S. Ostrach, Natural convection in enclosures, J. Heat Trans. 110 (1988) 1175–1190.

[23] J.A. Esfahani, V. Bordbar, Double diffusive natural convection heat transfer enhancement in a square enclosure using nanofluids, J. Nanotechnol. Eng. Med. 2 (2011) 021002.

[24] J. Rheinländer, Numerical calculation of heat and mass transfer in solar stills, Sol. Energy 28 (1982) 173–179.

[25] B. Djebedjian, M. Abou Rayan, Theoretical investigation on the performance prediction of solar still, Desalination 128 (2000) 139–145.

[26] E. Papanicolaou, V. Belessiotis, Patterns of double-diffusive natural convection with opposing buoyancy forces: Comparative study in asymmetric trapezoidal and equivalent rectangular enclosures, J. Heat Tran. (ASME) 130 (2008) 092501.1–092501.14.

[27] A. Omri, J. Orfi, S.B. Nasrallah, Natural convection effects in solar stills, Desalination 183 (2005) 173–178.

[28] K. Murase, H. Tobata, M. Ishikawa, S. Toyama, Experimental and numerical analysis of a tube-type networked solar still for desert technology, Desalination 190 (2006) 137–146.
[29] R. Chouikh, L. Ben Snoussi, A. Guizani, Numerical study of the heat and mass transfer in inclined glazing cavity: Application to a solar distillation cell, Renew. Energy 32 (2007) 1511–1524.
[30] R. Dunkle, Solar water distillation, The roof type still and a multiple effect diffusion still, in: Internat, Developments in Heat Transfer, ASME, Proc. Internat. Heat Transfer, Part V, University of Colorado, 1961, p. 895.
[31] R.S. Adhikari, A. Kumar, A. Kumar, Estimation of mass-transfer rates in solar stills, Int. J. Energy Res. 14 (1990) 737–744.
[32] S. Kumar, G.N. Tiwari, Estimation of convective mass transfer in solar distillation systems, Sol. Energy 57 (1996) 459–464.
[33] G.N. Tiwari, A. Minocha, P.B. Sharma, M. Emran Khan, Simulation of convective mass transfer in a solar distillation process, Energy Convers. Manage. 38 (1997) 761–770.
[34] M.A. Porta-Gándara, E. Rubio, J.L. Fernández, Experimental measurement of the water-to-cover heat transfer coefficient inside shallow solar stills, Appl. Therm. Eng. 18 (1998) 69–72.
[35] S. Aggarwal, G.N. Tiwari, Convective mass transfer in a double-condensing chamber and a conventional solar still, Desalination 115 (1998) 181–188.
[36] K. Voropoulos, E. Mathioulakis, V. Belessiotis, Transport phenomena and dynamic modeling in greenhouse-type solar stills, Desalination 129 (2000) 273–281.
[37] V.K. Dwivedi, G.N. Tiwari, Comparison of internal heat transfer coefficients in passive solar stills by different thermal models: An experimental validation, Desalination 246 (2009) 304–318.
[38] A.T. Shawaqfeh, M.M. Farid, New development in the theory of heat and mass transfer in solar stills, Sol. Energy 55 (1995) 527–535.
[39] J.A. Clark, The steady-state performance of a solar still, Sol. Energy 44 (1990) 43–49.
[40] Y.A. Cengel, Heat and Mass Transfer: A Practical Approach, third ed., McGraw-Hill, Singapore, 2006.
[41] R.V. Dunkl, CSIRO, Solar Water Distillation: The Roof Type Still and a Multiple Effect Diffusion Still, CSIRO, New York, NY, 1961.
[42] B.F. Sharpley, L.M.K. Boelter, Evaporation of water into quiet air from a one-foot diameter surface, Ind. Eng. Chem. 30 (1938) 1125–1131.
[43] P.T. Tsilingiris, Modeling heat and mass transport phenomena at higher temperatures in solar distillation systems—the Chilton–Colburn analogy, Sol. Energy 84 (2010) 308–317.
[44] M. Corcione, Effects of the thermal boundary conditions at the sidewalls upon natural convection in rectangular enclosures heated from below and cooled from above, Int. J. Therm. Sci. 42 (2003) 199–208.
[45] W.M. Kays, M.E. Crawford, B. Weigand, Convective Heat and Mass Transfer, fourth ed., McGraw-Hill, Singapore, 2005.
[46] P. Talukdar, C.R. Iskra, C.J. Simonson, Combined heat and mass transfer for laminar flow of moist air in a 3D rectangular duct: CFD simulation and validation with experimental data, Int. J. Heat Mass Transf. 51 (2008) 3091–3102.
[47] S.V. Patankar, Numerical Heat Transfer and Fluid Flow, Hemisphere, New York, NY, 1980.
[48] H.K. Versteeg, W. Malalasekera, An Introduction to Computational Fluid Dynamics: The Finite Volume Method, Prentice Hall, Glasgow, 2007.
[49] J.P. Holman, W.J. Gajda, Experimental Methods for Engineers, McGraw-Hill, New York, NY, 2001.